Journal of Power Sources 273 (2015) 1065–1072

Contents lists available at ScienceDirect

Journal of Power Sources

journal homepage: www.elsevier.com/locate/jpowsour

Enhanced Reduced Nicotinamide Adenine Dinucleotide electrocatalysis onto multi-walled carbon nanotubes-decorated gold nanoparticles and their use in hybrid biofuel cell

S. Aquino Neto [a, b], T.S. Almeida [a], D.M. Belnap [c], S.D. Minteer [b], A.R. De Andrade [a, *]

[a] Departamento de Química, Faculdade de Filosofia Ciências e Letras de Ribeirão Preto, Universidade de São Paulo, 14040-901 Ribeirão Preto, SP, Brazil
[b] Departments of Chemistry and Materials Science and Engineering, University of Utah, Salt Lake City, UT 84112, USA
[c] Departments of Biology and Biochemistry, University of Utah, Salt Lake City, UT 84112, USA

HIGHLIGHTS

- Au nanoparticles with smaller size shifts the oxidation potential of NADH.
- Four different protocol for Au nanoparticles synthesis are compared.
- All prepared catalysts catalyze NADH oxidation at low overpotentials.
- Efficient regeneration of NAD^+ led to higher power output.

GRAPHICAL ABSTRACT

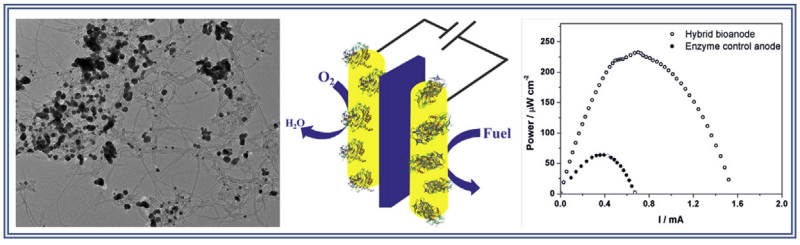

ARTICLE INFO

Article history:
Received 31 July 2014
Received in revised form
1 September 2014
Accepted 10 September 2014
Available online 5 October 2014

Keywords:
NADH electrocatalysis
Hybrid biofuel cell
Gold nanoparticles
Ethanol oxidation

ABSTRACT

We report the preparation of Au nanoparticles synthetized by different protocols and supported on the surface of multi-walled carbon nanotubes containing different functional groups, focusing on their electrochemical performance towards NADH oxidation, ethanol bioelectrocatalysis, and ethanol/O_2 biofuel cell. We describe four different synthesis protocols: microwave-assisted heating, water-in-oil, and dendrimer-encapsulated nanoparticles using acid or thiol species in the extraction step. The physical characterization of the metallic nanoparticles indicated that both the synthetic protocol as well as the type of functional groups on the carbon nanotubes affect the final particle size (varying from 13.4 to 2.4 nm) and their distribution onto the carbon surface. Moreover, the electrochemical data indicated that these two factors also influence their performance toward the electrooxidation of NADH. We observed that the samples containing Au nanoparticles with smaller size leads to higher catalytic currents and also shifts the oxidation potential of the targeted reaction, which varied from 0.13 to −0.06 V vs Ag/AgCl. Ethanol/O_2 biofuel cell tests indicated that the hybrid bioelectrodes containing smaller and better distributed Au nanoparticles on the surface of carbon nanotubes generates higher power output, confirming that the electrochemical regeneration of NAD^+ plays an important role in the overall biofuel cell performance.

1. Introduction

The incorporation of enzymes onto the surface of electrodes has recently become an attractive alternative in designing efficient energy conversion devices [1–3]. Bioelectronics such as biofuel cells make use of renewable and clean catalysts, afford selective

* Corresponding author. Tel.: +55 16 3602 3725; fax: +55 16 3633 8151.
E-mail addresses: ardandra@ffclrp.usp.br, adalgisa.andrade2@gmail.com (A.R. De Andrade).

http://dx.doi.org/10.1016/j.jpowsour.2014.09.074
0378-7753/

reactions, are able to catalyze the oxidation of a wide range of fuels, and can operate at low temperatures and near physiological pH [4]. From a large variety of enzymes being employed in enzymatic biofuel cells, NAD^+-dependent dehydrogenases represent one of the largest group of redox enzymes with potential application in many bioelectronic devices, mainly because of the low redox potential of the NADH/NAD^+ couple (0.09 V vs RHE) [2,5–7]. However, despite the high number of NAD^+-dependent dehydrogenase enzymes (over 300) and the commercial availability of many of these enzymes, a major drawback of applying these proteins in bioelectronics lies in the regeneration of NAD^+ species, which is an expensive cofactor [8]. The direct electrochemical regeneration of NAD^+ at conventional electrodes has poor kinetics and normally requires high overpotentials [9]; therefore, establishing a system that can efficiently electrochemically regenerate this is mandatory in order to achieve an efficient bioelectrode. In this context, literature has reported different strategies toward the electrochemical regeneration of NAD^+. Phenothiazine derivatives such as methylene green, methylene blue, and neutral red can efficiently oxidize NADH, even in their electropolymerized form [10–13]. Other materials such as metal oxides, poly(aniline), and enzymes have also been reported as efficient catalysts for the electrochemical regeneration of NAD^+ [14–16].

Despite the promising features of the biological fuel cells, ease and speed of electron transfer from the enzyme active site to the electrode surface, among others, are some of the crucial factors in the development of an economically viable energy conversion device [17]. In order to obtain better enzyme orientation, efficient electrical contact, and higher protein loading, recent biofuel cell literature proposes the incorporation of carbon nanomaterials into the bioelectrode structure. These materials have excellent electronic properties, high active surface area, and are friendly surfaces for biological molecules [3,18,19]. Another strategy to enhance the electronic conductivity through the bioelectrode surface is to incorporate metallic nanoparticles into their structure. Metallic nanoparticles have similar size as compared with some of the oxidoreductase enzymes employed in biofuel cells and highly active surface area, which can thus decrease the electron transfer distance and then facilitate this process at the bioelectrode surface [20]. Besides, this integration may lead to hybrid biological systems, with synergistic properties, improving the electrical contact and catalytic performance [21]. Moreover, regarding NADH oxidation, both carbon nanotubes and metallic nanoparticles have also been reported to assist NAD^+ regeneration by significantly lowering overpotentials [13,22–26].

In a previous report, we have investigated how hybrid nanostructured bioanodes containing enzymes and either Au, Pt, or $Pt_{0.75}Sn_{0.25}$ nanoparticles perform in an ethanol/O_2 biofuel cell [27]. Our results indicated that the introduction of metallic nanoparticles into the bioanode structure enhances the overall biofuel cell performance. From the different nanocatalysts tested, the bioelectrode containing Au nanoparticles displayed the best performance, which was related to the catalytic behavior of this material towards NADH. In fact, the Au nanoparticles supported on MWCNTs were able to shift the oxidation peaks by almost 200 mV vs Ag/AgCl toward negative potentials when compared to a well-known NADH catalyst, poly(methylene green). Considering the previously obtained data and the importance of the reaction of NAD^+ regeneration in the field of bioelectrocatalysis, the present paper has focused on improvements in the Au nanoparticles synthesis protocol. The goal was to achieve nanocatalysts with smaller nanoparticles size and evaluate how they behave on carbon nanotubes containing different functional groups. The electrochemical performance towards NADH oxidation as well as ethanol bioelectrocatalysis in an ethanol/O_2 biofuel cell tests are presented.

2. Material and methods

2.1. Chemicals

All reagents were of analytical grade and used without further purification. PAMAM dendrimer, ethylenediamine core, generation 4.0 solution; $HAuCl_4$; Nafion® 1100 EW 5% by wt. suspension; Nafion® NRE212; the coenzyme NAD^+; and the enzyme alcohol dehydrogenase (ADH, obtained from *Saccharomyces cerevisiae* lyophilized powder, E.C. 1.1.1.1, initial activity of 331 Units mg^{-1}, where one enzyme unit, *U*, is defined by the ability to produce 1 μmol of NADH per minute) were purchased from Sigma–Aldrich and used as received. Multi walled carbon nanotubes (MWCNTs, OD 20–30 nm, ID 5–10 nm, OL 10–30 μm), COOH-functionalized MWCNTs (OD ≤ 8 nm, ID = 2–5 nm, OL = 10–30 μm), and NH_2-functionalyzed MWCNTs (OD < 20 nm, ID = 4 nm, OL = 1–12 μm) were acquired from Cheaptubes.com. All the solutions were prepared with high-purity water from a Millipore Milli-Q system. pH was measured using a pH electrode coupled to a Qualxtron model 8010 pH meter. All the enzyme and coenzyme solutions were freshly prepared and used immediately.

2.2. Metallic nanoparticles synthesis

Four different synthesis protocols were employed to obtain Au particles with nanometric dimensions: microwave-assisted heating (named protocol #1), water-in-oil (named protocol #2), dendrimer-encapsulated nanoparticles using acid extraction (named protocol #3), and dendrimer-encapsulated nanoparticles using thiol extraction (named protocol #4), which were prepared as follows. For the preparation of Au nanoparticles using the protocol #1, the nanocatalyst was prepared with a 40 wt. % metal loading by supporting the metallic nanoparticles onto carbon nanotubes with different functional groups e.g., MWCNTs, COOH-MWCNT, and NH_2-MWCNTs. Briefly, the catalysts were obtained by dissolving sodium citrate at a 1:5 M ratio in 25 mL of propylene glycol [28]. After that, 0.10 mol L^{-1} $HAuCl_4$ aqueous solutions were added to the mixture. Then, the solution was stirred in an ultrasonic bath for 2 min, followed by the addition of each MWCNTs to achieve catalysts with the desired carbon/metal loading. The mixture was kept under ultrasonic stirring for 10 min to obtain a homogeneous suspension. This suspension was placed in a common household microwave oven (Panasonic® NN-ST568WRU, 2450 Hz, 800 W) operating at a power of 800 W for 5 min. The final suspension was filtered and exhaustively washed with water. The solid product was dried at 120 °C for 2 h under N_2 atmosphere.

The Au nanoparticles synthesized in a water-in-oil microemulsion of water/poly(ethyleneglycol)-dodecylether (BRIJ 30)/n-heptane followed a protocol similar to what was described in literature [29,30]. Briefly, 40 wt. % metal loading metallic nanoparticles was supported onto non-functionalized MWCNTs. Water/surfactant molar ratio was kept constant at 3.8. After addition of proper amount of 0.10 mol L^{-1} $HAuCl_4$, a 15 M excess $NaBH_4$ was added to the mix followed by the addition of the MWCNTs. The catalyst was then filtered and washed with acetone. The solid product was dried at 120 °C for 2 h under N_2 atmosphere.

For the preparation of the dendrimer-encapsulated Au nanoparticles, the synthesis involves a sequential two-step reactions. First, the metallic species are stabilized onto the NH_2-functionalized PAMAM structure; then, a strong reducing agent, such as $NaNH_4$, is added to the mixture, which consequently causes formation of the encapsulated Au nanoparticles [31]. Briefly, 30 mL of an aqueous solution containing 0.8 mmol L^{-1} PAMAM dendrimers and 55 equiv of 0.1 mol L^{-1} $HAuCl_4$ was kept under stirring for 15 min; after that, a fivefold molar excess of $NaBH_4$ was added, the pH was adjusted to

10, and the mixture was kept under stirring for 2 h. The initial pale yellow solution changed to a very intense red color, characteristic of the Au metallic nanoparticles, at the end of the reaction [32]. To extract and support the Au metallic nanoparticles onto the surface of the carbon nanotubes, two different strategies were employed. The amine groups of the PAMAM dendrimer have different pKa's; in fact, the surface primary amines are more basic (pKa = 9.23) than the internal tertiary amines (pKa = 6.30) [33]. Thus, one can control trapping metal ions to primary amine groups on the periphery by keeping a basic pH. Based on this characteristic, the first strategy (protocol #3) to extract the metallic species is to lower the pH solution after the nanoparticle encapsulation step. To this end, the proper amount of MWCNTs was added to the dendrimer-encapsulated nanoparticles solution, the pH was adjusted to 3 and the mixture was kept under stirring overnight, followed by filtration and drying. The second strategy (protocol #4) was to use thiol species to extract the metallic species from the dendrimer structure [34]. The protocol involves the addition of an organic phase containing *n*-alkanethiols, which self-assemble onto the surface of the encapsulated metal nanoparticles, extract them from the dendrimers structure carrying it to the toluene phase and leaving the dendrimer in the aqueous phase [34]. Alternatively from the other protocols, protocol #4 was only effective with diluted solutions, so in this case, a 2 wt. % metal loading was prepared. Briefly, after the preparation of the dendrimers encapsulated nanoparticles, 10 mL of 20 mM *n*-dodecanethiol solution in n-heptane were added, and the mixture was shaked for 15 min. The organic phase was separated and evaporated to a final volume of 2 mL. Then, 15 mL of ethanol was added along with non-functionalized MWCNTs and stirred overnight, followed by filtration and drying. All the experimental metal loading achieved with the different protocols employed are presented in Table 1.

2.3. Nanoparticles physical characterization

Diffraction patterns of the freshly prepared metallic nanoparticles as function of the different protocols employed were obtained with an X-ray diffractometer (D5005 Siemens) operating with Cu Kα radiation ($\lambda = 1.5406$ Å) generated at 40 kV and 40 mA. The following parameters were kept constant during the analysis: 2θ range = 20°–90°, step = 0.03° s^{-1}, and total analysis time = 1.97 h. The phase composition of the nanocatalyst and the position relative to the Kα1 monochromatic radiation were achieved by fitting the experimental angular range of interest to the pseudo-Voigt function per crystalline peak using the Profile Plus Executable refinement program (Siemens AG). The crystallite size value was calculated using the Debye–Scherrer equation [35]. The morphology of the Au nanoparticles supported on MWCNTs was also investigated by transmission electron microscopy (TEM). A few microliters (approximately 3.5 μL) of each Au-MWCNT sample (dissolved in ethanol) was placed on a carbon-Formar-coated, Cu-mesh TEM grid. After drying, the specimen was placed in the microscope and imaged. Images were recorded on a FEI Tecnai F20 transmission electron microscope operated at 200 kV with a FEI Eagle CCD (charge-coupled device) camera.

Table 1
Au nanoparticles sizes, NADH oxidation peak potential, and maximum power density achieved in the ethanol/O_2 biofuel cell tests as a function of different synthesis protocols.

Au nanoparticle synthesis protocol	Crystallite size/nm	Experimental metal loading/%	NADH oxidation peak/V vs Ag/AgCl	Maximum power density/μW cm^{-2}
Protocol#1_MWCNTs	13.4	38	0.13	171 ± 9
Protocol#1_COOH-MWCNTs	12.4	37	0.09	166 ± 8
Protocol#1_NH_2-MWCNTs	9.6	39	−0.06	226 ± 12
Protocol#2_MWCNTs	4.9	33	0.08	201 ± 10
Protocol#3_MWCNTs	3.7	32	0.06	198 ± 9
Protocol#4_MWCNTs	2.4	2	0.04	175 ± 9

2.4. NADH cyclic voltammetry

Cyclic voltammetry experiments were performed to evaluate the ability of the prepared nanoparticles to regenerate NAD^+ species. The assays were conducted in 0.1 mol L^{-1} phosphate buffer, pH 7.2, containing 0.1 mol L^{-1} sodium nitrate and different concentrations of β-NADH in a single compartment cell. The sweeps were registered from −0.30 V to 0.30 V vs Ag/AgCl at 0.010 V s^{-1} using a potentiostat/galvanostat Autolab (SPGSTAT30). The working electrode samples consisted of 0.071 cm^2 glassy carbon electrodes containing only the metallic nanoparticles supported onto MWCNTs. The samples were prepared by adding 3 μL of an ethanolic dispersion containing 5 mg mL^{-1} of the different prepared Au nanoparticles onto the carbon support, followed by drying. A spiraled platinized platinum wire (15 cm) served as the counter electrode and a homemade Ag/AgCl, sat. KCl (+0.199 V relative to hydrogen standard electrode) was used as the reference electrode. Chronoamperometric tests were conducted with consecutive addition of NADH at a fixed oxidation potential (50 mV larger than the NADH oxidation peak potential). All experiments were performed in triplicate and uncertainties correspond to one standard deviation.

2.5. Bioanode preparation and characterization

Using a 1 cm^2 carbon cloth platform (HT1400W, ELAT® GDL – BASF) as the electrode support containing a electropolymerized thin stable poly(methylene green) film [11], the hybrid bioelectrode architecture was achieved by immobilizing the enzymes on top of an electrocatalyst layer containing the different metallic nanoparticles. To this end, 50 μL of an ethanolic dispersion containing 5 mg mL^{-1} of the different prepared Au nanoparticles were added onto the carbon support, followed by drying. After that, the enzymes were immobilized with TBAB-modified Nafion® encapsulation technique, as per the procedure described in Ref. [36]. The modified polymer was prepared as described previously and the enzymes were immobilized by adding 50 μL of a 1:2 enzyme/polymer ratio in phosphate buffer solution (pH 7.2) containing 1.9 mmol L^{-1} NAD^+, directly onto the carbon cloth.

For the biofuel cell tests, current density were measured in a single compartment cell separated by a Nafion® membrane. A gas diffusion membrane (ELAT) consisting of platinum 20% on vulcanized carbon (E-TEK) hot pressed to a Nafion® membrane was used as the cathode. The cathode side was kept in direct contact with air. The cell compartment (10 mL) was filled with phosphate buffer (pH 7.2), 1.9 mmol L^{-1} NAD^+, 0.1 mol L^{-1} sodium nitrate, and 0.1 mol L^{-1} ethanol. The assays were conducted at room temperature (25 ± 1 °C) and the potential was controlled by a PAR Potentiostat/Galvanostat Model 273A. The OCV was measured for 1 h; quasi-stationary linear voltammetry was recorded at a scan rate of 1 mV s^{-1}. The power density was calculated from the obtained data. All the results are based on the measurement of triplicate electrodes.

3. Results and discussion

3.1. Physical characterization of Au nanoparticles

The crystalline structure as well as the crystallite size of the Au nanoparticles were determined for each synthetic protocol

employed. Based on the diffraction patterns obtained with the freshly prepared samples (Supplementary material), all of the metallic nanoparticles supported onto MWCNTs displayed a FCC crystalline structure. Considering the crystallite size calculated using the Debye–Scherrer equation, the results indicated that there is a direct relationship between the synthetic protocol employed and the final crystallite size achieved. Table 1 summarizes the obtained data. For the samples prepared with the microwave-assisted heating protocol, the determined size was of 13.4, 12.4, and 9.6 nm for the nanoparticles supported onto regular MWCNTs, COOH-functionalized MWCNTs, and NH_2-functionalized MWCNTs, respectively. Based on the obtained data, the stabilization provided by the amine groups contained in the nanotubes accounts for the slightly smaller size achieved in this sample when compared to the other tested carbon materials. Considering the sample prepared by protocol #2, synthetized in a water-in-oil microemulsion, X-ray analysis indicated that the Au nanoparticles displayed almost half of the size, 4.9 nm, when compared to the results achieved with the microwave-assisted heating protocol. This data is also similar to the size reported in literature employing similar synthetic protocol [30]. Regarding the size determined for Au nanoparticles samples synthetized with the assistance of PAMAM dendrimers, both protocols provided the smallest nanoparticles, with determined size of 3.7 and 2.4 nm for the sample protocols #3 and #4, respectively. This data can be predicted considering the different stabilizing agents present in each protocol, i.e.: the highly NH_2-functionalized and well-defined small porous structure of PAMAM dendrimers are able to more efficiently stabilize the Au nanoparticles during the synthesis and consequently provide the smallest nanoparticles size.

To gain insights into the dispersion of the Au nanoparticles along the MWCNTs surface, TEM images were obtained for each sample prepared. Fig. 1 depicts TEM images of the Au nanoparticles synthetized by the microwave-assisted heating protocol (protocol #1), either supported onto untreated MWCNTs (Fig. 1A), COOH-functionalized MWCNTs (Fig. 1B), or NH_2-functionalized MWCNTs (Fig. 1C). The images reveal that similarly to the behavior observed in X-ray analysis (in which the samples prepared with NH_2-MWCNTs provided better nanoparticle stabilization and consequently smaller size), a better Au nanoparticle distribution along the carbon nanotubes is observed in the sample prepared with NH_2-functionalized MWCNTs as a result of better stabilization and consequently smaller particle size. For the other two samples prepared by protocol #1, higher agglomeration are observed in both cases and the acid-functionalized sample led to larger aggregates. Considering the different methodologies employed, Fig. 1D, E, and F indicates that both the sample synthetized by the water-in-oil protocol (protocol #2) as well as the sample achieved with nanoparticles encapsulation in PAMAM dendrimers (protocols #3 and #4) and further extraction and supporting on MWCNTs provided more homogeneous and better-distributed Au nanoparticles through the surface of the nanotubes, when compared with the microwave-assisted heating protocol. Moreover, the lower amount of dark spots along the nanotubes matrix in Fig. 1F corroborates the 2 wt. % metal loading obtained with this sample. The obtained image profile confirms that the water-in-oil methodology, in which the nanosized droplets in the aqueous phase is surrounded by a monolayer of surfactant molecules of the organic phase, provided better stabilization of the metallic nanoparticles compared to the citrate molecules used in the microwave-assisted heating

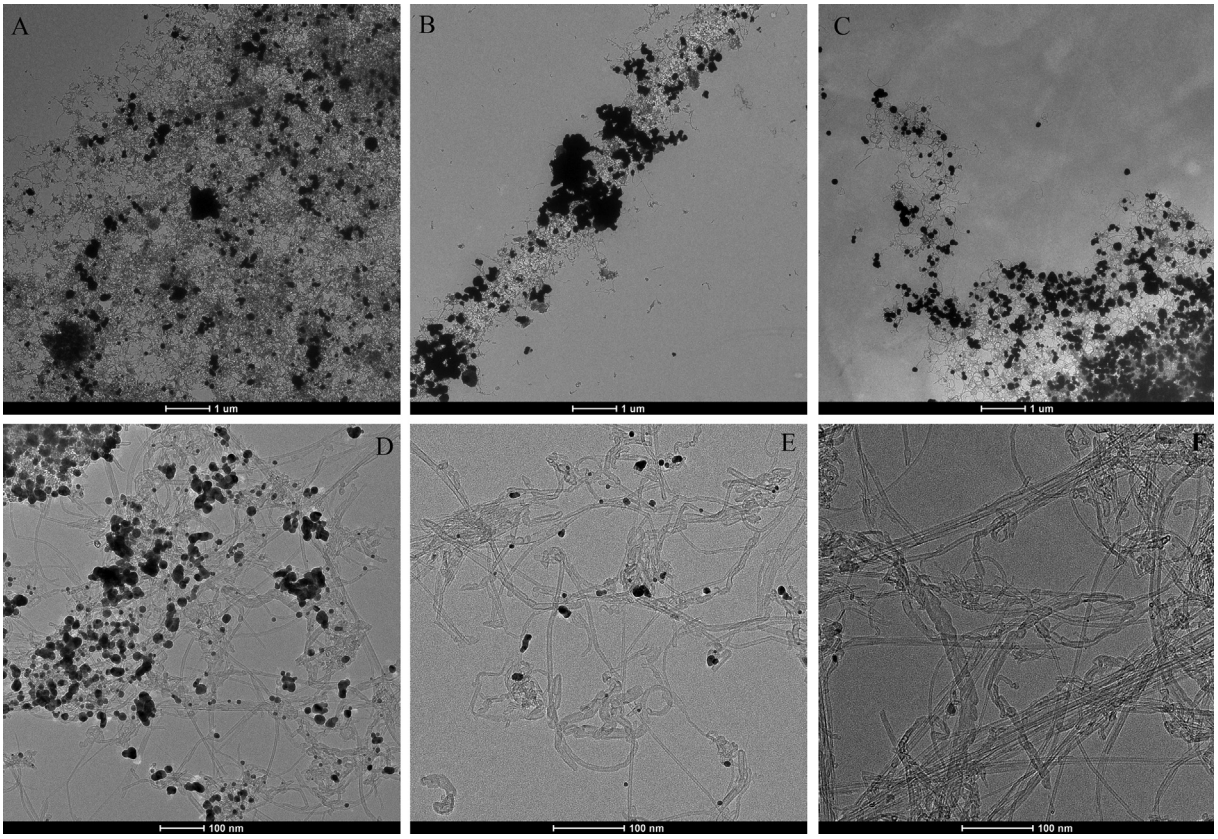

Fig. 1. TEM images of the freshly prepared Au nanoparticles synthetized by the microwave-assisted heating protocol (protocol #1), either supported onto untreated MWCNTs (A), COOH-functionalized MWCNTs (B), and NH_2-functionalized MWCNTs (C). D, E, and F represent the images obtained for the samples synthetized by protocols #2 (D), #3 (E), and #4 (F), all supported on non-functionalized regular MWCNTs.

methodology, while the highly functionalized and well-defined porous structure of PAMAM dendrimers generated both the smaller particles size and better particle distribution.

3.2. NADH cyclic voltammetry and ethanol/O_2 biofuel cell tests

3.2.1. NADH electrocatalysis on Au nanoparticles

The electrochemical regeneration of NAD^+ via the oxidation of NADH species formed in the enzymatic catalyzed reaction is of great importance to obtain high current bioelectrodes employing NAD^+-dependent dehydrogenase enzymes. However, in the absence of an electrocatalyst, this reaction occurs at overpotentials above 1 V on carbon materials [37]; therefore, achieving NADH oxidation at lower potentials is mandatory to obtain efficient bioelectronics such as biosensors and biofuel cells. In order to evaluate how efficient the Au nanoparticles catalyze the targeted NADH oxidation reaction, cyclic voltammetric experiments were performed with the freshly prepared catalysts. Fig. 2 shows the representative cyclic voltammograms achieved with the Au nanoparticles prepared by the microwave-assisted heating protocol, either supported onto untreated MWCNTs (Fig. 2A), COOH-functionalized MWCNTs (Fig. 2B), and NH_2-functionalized MWCNTs (Fig. 2C) in 1 mmol L^{-1} β-NAD-reduced dipotassium salt solution in pH 7.2 phosphate buffer.

Analysis of Fig. 2 reveals that all the Au nanoparticles supported on different functionalized MWCNTs prepared by protocol #1 display well-defined oxidation peaks towards NADH. The cyclic voltammograms obtained indicate that there is a direct effect of the functional groups present in the surface of each carbon nanotube and the final performance of the metallic nanoparticles. In fact, the sample containing the Au nanoparticles supported on the surface of NH_2-functionalyzed MWCNTs displayed significant low overpotential for NADH oxidation. In this case, the obtained oxidation peak lied at −0.06 V vs Ag/AgCl. For the other two samples, the obtained oxidation peak stayed at 0.13 V vs Ag/AgCl for the Au nanoparticles supported on regular MWCNTs and a less intense peak at 0.09 V vs Ag/AgCl was achieved with the sample supported on COOH-functionalized MWCNTs. Taking into account the physical characterization of the Au nanoparticles prepared via microwave-assisted heating protocol along with the electrochemical data achieved with each sample, one can clearly infer that the metallic nanoparticle size and distribution along the carbon nanotubes surface play an important role in the overall performance of the metal catalyst. Indeed, the sample containing the Au nanoparticles supported on NH_2-functionalyzed MWCNTs displayed the smaller size and better distribution among the sample prepared via protocol #1 and consequently provided the lower NADH overpotential. In fact, the results point to an oxidation peak shift around 150 and 190 mV vs Ag/AgCl for the sample supported on NH_2-functionalyzed MWCNTs when compared to the other two nanotubes samples, respectively, which represents a very significant improvement in terms of the energy required to perform the target reaction. Moreover, another consideration to be made about the obtained cyclic voltammograms as a function of the different functionalized carbon nanotubes is that, surprisingly, NH_2-rich MWCNTs itself display a catalytic behavior toward NADH at significant low potential, in fact an oxidation peak at 0.23 V vs Ag/AgCl was attained. Literature has shown that NADH can be oxidized at MWCNTs films prepared via a covalent layer-by-layer deposition of both aminated-MWCNTs and carboxylated-MWCNTs [38]. Plus, it has also been shown that nitrogen-doped carbon nanotubes improve NADH oxidation [39]. Moreover, different MWCNT/polymer composites

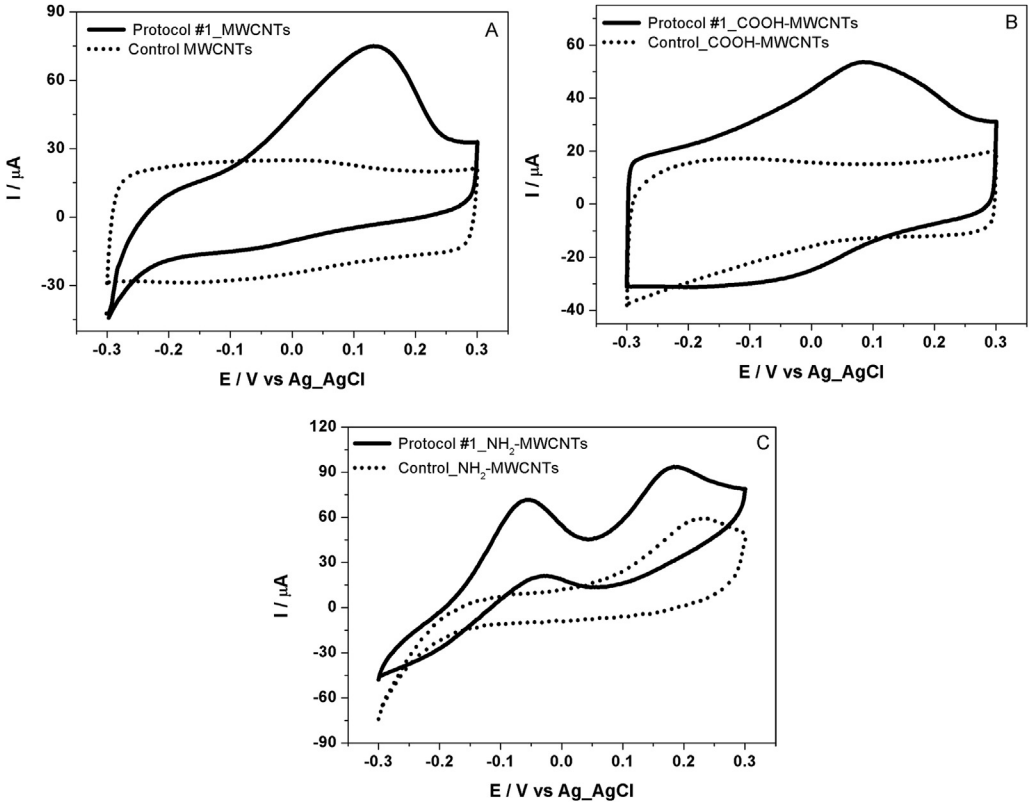

Fig. 2. Representative cyclic voltammograms of NADH with different MWCNTs-decorated Au nanoparticles prepared by the microwave-assisted heating protocol (protocol #1), either supported onto untreated MWCNTs (A), COOH-functionalized MWCNTs (B), and NH_2-functionalized MWCNTs (C) in phosphate buffer, pH 7.2 containing 1 mmol L^{-1} β-NADH-reduced dipotassium salt and 0.1 mol L^{-1} sodium nitrate, $\nu = 0.01$ V s^{-1}.

have also been able to catalyze this reaction [40]. The mechanism involved in the NADH oxidation at the surface of carbon nanotubes is not certain, and in some situations, it is hypothesized that oxygen and quinone moieties can improve the electron transfer and consequently facilitate the oxidation reaction [24,40]. Considering the data obtained in this study, we believe that the lone pairs of electrons of the amines groups can interact with the sidewalls of the carbon nanotubes and change their electronic properties, thus providing the catalytic effect of the NH_2-functionalyzed MWCNTs sample toward NADH.

Although the results showed that the NH_2-functionalized MWCNTs was the best matrix to support the Au gold nanoparticles using protocol #1, unfortunately, the synthesis using this material was not successful with the protocols employing PAMAM dendrimer, thence, the study of different synthetic protocols was carried out using a non-functionalized matrix which was effective with all the different proposed protocols. Accordingly, in order to evaluate the effect of the different synthetic protocols employed for Au nanoparticle preparation towards NADH oxidation, cyclic voltammetry experiments were carried out for each different catalyst sample, always supporting the metallic species on non-functionalized MWCNTs (Fig. 3A). The electrochemical behavior encountered in a 1 mmol L^{-1} NADH solution in pH 7.2 phosphate buffer reveals that the catalytic behavior of Au nanoparticles towards NADH oxidation follows a similar path as observed in the study as a function of different functionalized MWCNTs discussed above (i.e, nanoparticle size and distribution along the MWCNTs surface direct influence their catalytic behavior toward NADH). The obtained data indicated that both smaller size particles and better distribution lead to a lower overpotential towards NADH oxidation. In fact, an almost 90 mV shift is observed when we compare the oxidation peaks achieved with the Au nanoparticles prepared by microwaved-assisted heating and the sample prepared via dendrimer-encapsulated nanoparticles using thiol extraction.

The determined oxidation peaks potential towards NADH oxidation as a function of different protocols were of respectively 0.13, 0.08, 0.06, and 0.04 V vs Ag/AgCl for protocols #1, #2, #3, and #4, respectively. Accordingly, if we compare the potential peaks obtained for each sample with their nanoparticle size determined by X-ray analysis, a direct relation between these values can be observed (i.e., the Au nanoparticles supported on MWCNTs via protocol 4 displayed the smaller size and consequently provided the lower overpotential for the targeted reaction). Considering the cyclic voltammograms obtained with the samples prepared by protocol #1, #2, and #3, the slightly higher current observed with protocol #1 should be associated with the higher experimental metal loading achieved in this case (Table 1); i.e., a higher quantity of Au led to a slightly higher current in the NADH cyclic voltammogram. Interestingly, besides having the smaller particle size, the sample prepared by protocol #4 also had a much lower amount of metallic species (2 wt. % metal loading against up to 38 wt. % metal loading of the other samples). It is expected that an increase in the amount of the electrocatalyst will provide a higher area of contact with NADH species and consequently an increase in the catalytic current. Nevertheless, the sample prepared by protocol #4, which contains the lower amount of metal nanoparticles but with smaller size (or larger surface area), displayed the higher catalytic peak. Besides, we also observed that this sample does not lead only to higher catalytic current, in fact, the electrochemical data indicated that lower overpotentials towards NADH oxidation was attained in this case. Taking into account both physical characterization and all the electrochemical data achieved with the samples supported on different functionalized carbon nanotubes and prepared by different synthesis protocols, we can hypothesize that not only the quantity of Au, but both smaller nanoparticle size and better distribution of these metallic species along the surface of the MWCNTs provides a more favorable condition for the occurrence of the reaction of NADH oxidation, with consequently lower overpotential observed in the cyclic voltammograms. The results presented here are significant in terms of the energy required to perform the targeted reaction when we compare it to a well-known NADH catalyst, poly(methylene green) [13,41]. We verified that our best NADH catalyst (Au nanoparticles prepared by protocol #4) supported on the same type of matrix, besides displaying a well-defined oxidation peak toward NADH oxidation, shifted the oxidation potential by more than 200 mV vs Ag/AgCl toward negative potentials. Moreover, this catalyst was prepared with a much lower amount of Au, which is very important considering the high cost of the noble metal employed. In order to confirm the efficiency of the Au nanoparticles-based catalyst to electrooxidize NADH, we also carried out chronoamperometric assay with consecutive addition of NADH at a fixed potential of 50 mV larger than the NADH oxidation peak potential. Fig. 3B confirms that the prepared nanoparticles supported on MWCNTs are able to regenerate NAD^+ even at low concentrations, and catalysis can be verified by the linear increase in the catalytic current with NADH additions.

3.2.2. *Ethanol/O_2 biofuel cell evaluation*

Considering the improvement in biofuel cell performance afforded by the use of hybrid bioelectrodes containing Au nanoparticles, one can hypothesize that the metallic species can enhance either the catalytic rate or the electron transfer process.

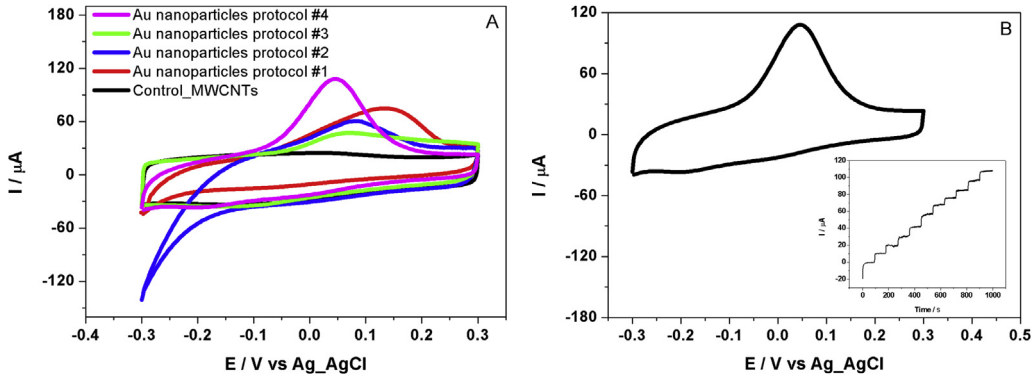

Fig. 3. (A) Representative cyclic voltammograms of NADH 1 mmol L^{-1} with different MWCNTs-decorated Au nanoparticles prepared by different synthesis protocols, supported on non-functionalized MWCNT. (B) Cyclic voltammogram of NADH 1 mmol L^{-1} with MWCNTs-decorated Au nanoparticles prepared by protocol #4. In set: chronoamperometric test with MWCNTs-decorated Au nanoparticles prepared by protocol #4 with consecutive addition of NADH at fixed potential of 50 mV larger than the NADH oxidation peak potential, in pH 7.2 phosphate buffer and 1 mmol L^{-1} sodium nitrate.

However, in the case of bioelectrodes employing NAD^+-dependent enzymes, we have observed that the catalytic effect toward the electrochemical regeneration of NAD^+ plays an important role in the overall biofuel cell performance [27]. Therefore, in order to evaluate the effect of the Au nanoparticles prepared by different synthesis protocols at the final performance of the hybrid bioelectrodes, biofuel cell tests were performed with each of the fresh prepared bioelectrodes containing the metallic species. Table 1 summarizes all the experimental parameters achieved with the hybrid bioelectrodes prepared by different synthesis protocols, including the maximum power density achieved in each biofuel cell test, the crystallite size of the Au nanoparticles achieved in each case, as well as their oxidation peak potential toward NADH.

The power density behavior obtained with the Au hybrid bioelectrodes can be understood if both the physical characterization and NADH electrochemical data are taken into account. The obtained data indicated that when the Au nanoparticles are smaller and better distributed onto the surface of carbon nanotubes, more easily is the regeneration of NAD^+ and consequently higher is the output power generated by the hybrid bioelectrodes. Besides, the quantity of Au nanoparticles in each bioelectrode also accounts for the final power performance. Considering the different protocols and different carbon nanotubes samples, the best power performance achieved with the sample prepared by protocol #1 with the Au nanoparticles supported on NH_2-functionalized MWCNTs can be understood considering that this electrode displayed the highest ability to regenerate NAD^+ species (two well-defined catalytic peaks towards NADH at −0.06 and 0.23 V vs Ag/AgCl) and as stated before, this plays an important role in the overall performance of NAD^+-dependent bioelectrodes. Fig. 4 show representative power curves obtained in the biofuel cell tests employing the hybrid bioanode prepared by protocol #1 with the Au nanoparticles supported on NH_2-functionalized MWCNTs as well as a control sample containing enzyme and MWCNTs only.

Moreover, the power density data presented in Table 1 also indicated that the effect of metal loading has also influence on the final performance of the hybrid bioelectrodes. In fact, the sample prepared by protocol #4 (which furnished the Au nanoparticles with smaller size) generated the smaller power density value, which should be related with the lower amount of metallic species supported in this case. However, if the obtained power curves were normalized by the theoretical Au NPs surface area deposited in each sample, clearly the sample synthetized by protocol #4 would display the higher intrinsic output power. In fact, based on the X-ray diffraction patterns and the determined particles sizes, the estimated Au nanoparticles surface area for each hybrid bioelectrode as a function of the different protocols is 22, 23, 31, 52, 67, 6.5 cm^2, for protocols #1-MWCNTs, #1-MWCNTs_COOH, #1-MWCNT_NH_2, #2, #3, and #4, respectively (Supplementary material). From an economic perspective, when one take these values into consideration, the use of a protocol that makes use of smaller quantity of an expensive material (Au) in bioelectrode preparation, but at the same time generate reasonable power, becomes quite interesting.

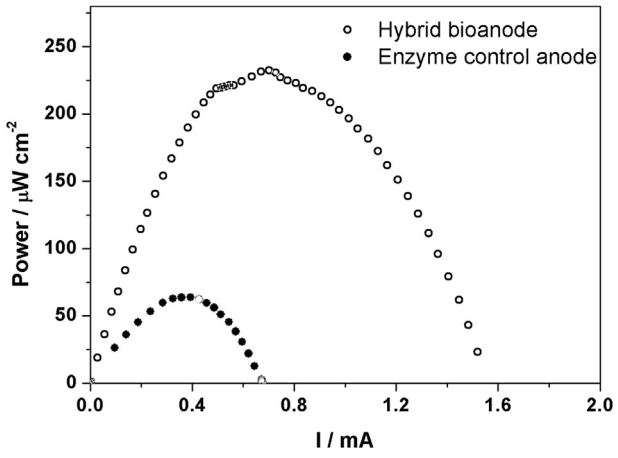

Fig. 4. Representative power density curves obtained in the ethanol/O_2 biofuel cell tests employing the hybrid bioanode prepared by protocol #1 with the Au nanoparticles supported on NH_2-functionalized MWCNTs. Phosphate buffer (pH 7.2), 1.9 mmol L^{-1} NAD^+, and 100 mmol L^{-1} ethanol.

Overall, when taken together, NADH electrochemical data along with the biofuel cell tests of all the Au-based hybrid bioelectrodes prepared here show that the introduction of small amount of Au nanoparticles is a good strategy to obtain efficient bioanodes for ethanol/O_2 enzymatic biofuel cells employing NAD^+-dependent enzymes. Besides, it opens the possibility to employ this architecture for other biotechnological purposes employing NAD^+-dependent enzymes, such as electrosynthesis and biosensors.

4. Conclusions

All the four different synthesis protocols employed proved to be efficient for obtaining Au particles with nanometric dimensions. From the different strategies attempted, we must highlight that, to our knowledge, this is the first description of synthesis of dendrimer encapsulated nanoparticles with effective support onto the surface of carbon nanotubes. Our results indicated that the synthesis protocol as well as the type of the functional groups present onto the surface of the carbon nanotubes direct influence the final crystallite size of the synthetized nanoparticles and their distribution at the carbon support. The electrochemical characterization of the Au nanoparticles supported on the surface of different functionalized MWCNTs and synthetized by different protocols showed that independently of the procedure employed, they were all capable of catalyzing the NADH oxidation at low overpotentials. Besides, we have shown that the crystallite size of the synthetized nanoparticles and their distribution along the surface of the carbon nanotubes influence the NADH oxidation behavior; in fact, smaller crystallite particle size and better distribution lead not only to higher catalytic currents but also to shift in the oxidation potential of the targeted reaction. The results also showed that in the case of the protocol using thiol species in the Au nanoparticles extraction step, an efficient catalyst was achieved with very low amount of small and dispersed metallic species. The electrochemical data presented is significant in terms of the energy required to perform the targeted reaction when we compare the obtained values to a well-known NADH catalyst, methylene green, where it is observed a potential shift of more than 200 mV vs Ag/AgCl toward negative potentials. Finally, the ethanol/O_2 biofuel cell tests showed that smaller and better distributed Au nanoparticles led not only to a more efficient regeneration of NAD^+ species, but also to higher power output generated by the hybrid bioelectrodes. The best power performance was obtained with the hybrid bioelectrode containing the Au nanoparticles supported on NH_2-functionalized MWCNTs, which also displayed the highest ability to regenerate NAD^+ species.

Acknowledgments

Financial support from FAPESP (Grant 2012/10667-0 and 2014/00536-0), CAPES, and CNPq are gratefully acknowledged. The authors also thank the National Science Foundation (Grant # 1057597).

Appendix A. Supplementary data

Supplementary data related to this article can be found at http://dx.doi.org/10.1016/j.jpowsour.2014.09.074.

References

[1] I. Ivanov, T. Vidaković-Koch, K. Sundmacher, Energies 3 (2010) 803–846.
[2] M.H. Osman, A.A. Shah, F.C. Walsh, Biosens. Bioelectron. 26 (2011) 3087–3102.
[3] S.D. Minteer, P. Atanassov, H.R. Luckarift, G.R. Johnson, Mater. Today 15 (2012) 166–173.
[4] R.A. Bullen, T.C. Arnot, J.B. Lakeman, F.C. Walsh, Biosens. Bioelectron. 21 (2006) 2015–2045.
[5] M.T. Meredith, S.D. Minteer, Annu. Rev. Anal. Chem. 5 (2012) 157–179.
[6] H. Li, K.E. Worley, S. Calabrese Barton, ACS Catal. 2 (2012) 2572–2576.
[7] C.M. Halliwell, E. Simon, C.-S. Toh, A.E.G. Cass, P.N. Bartlett, Bioelectrochemistry 55 (2002) 21–23.
[8] L. Gorton, E. Domínguez, in: Encyclopedia of Electrochemistry, Wiley-VCH Verlag GmbH & Co. KGaA, 2007.
[9] A.A. Karyakin, E.E. Karyakina, W. Schuhmann, H.-L. Schmidt, Electroanalysis 11 (1999) 553–557.
[10] A.E. Blackwell, M.J. Moehlenbrock, J.R. Worsham, S.D. Minteer, J. Nanosci. Nanotechnol. 9 (2009) 1714–1721.
[11] Z. Dong-mei, F. Hui-Qun, C. Hong-yuan, J. Huang-xian, W. Yun, Anal. Chim. Acta 329 (1996) 41–48.
[12] H. Li, H. Wen, S. Calabrese Barton, Electroanalysis 24 (2012) 398–406.
[13] S. Aquino Neto, T.S. Almeida, M.T. Meredith, S.D. Minteer, A.R. De Andrade, Electroanalysis 25 (2013) 2394–2402.
[14] Y.H. Kim, Y.J. Yoo, Enzyme Microb. Technol. 44 (2009) 129–134.
[15] P.N. Bartlett, P.R. Birkin, E.N.K. Wallace, J. Chem. Soc. Faraday Trans. 93 (1997) 1951–1960.
[16] G.T.R. Palmore, H. Bertschy, S.H. Bergens, G.M. Whitesides, J. Electroanal. Chem. 443 (1998) 155–161.
[17] D. Leech, P. Kavanagh, W. Schuhmann, Electrochim. Acta 84 (2012) 223–234.
[18] M. Falk, Z. Blum, S. Shleev, Electrochim. Acta 82 (2012) 191–202.
[19] W. Feng, P. Ji, Biotechnol. Adv. 29 (2011) 889–895.
[20] K.A. Vincent, X. Li, C.F. Blanford, N.A. Belsey, J.H. Weiner, F.A. Armstrong, Nat. Chem. Biol. 3 (2007) 761–762.
[21] X.-Y. Yang, G. Tian, N. Jiang, B.-L. Su, Energy Environ. Sci. 5 (2012) 5540–5563.
[22] M.T. Meredith, F. Giroud, S.D. Minteer, Electrochim. Acta 72 (2012) 207–214.
[23] Y.Y. Sun, Q.X. Ren, X. Liu, S. Zhao, Y. Qin, Biosens. Bioelectron. 39 (2013) 289–295.
[24] M. Musameh, J. Wang, A. Merkoci, Y. Lin, Electrochem. Commun. 4 (2002) 743–746.
[25] H. Chang, X. Wu, C. Wu, Y. Chen, H. Jiang, X. Wang, Analyst 136 (2011) 2735–2740.
[26] C.R. Raj, B.K. Jena, Chem. Commun. (2005) 2005–2007.
[27] S. Aquino Neto, T.S. Almeida, L.M. Palma, S.D. Minteer, A.R. de Andrade, J. Power Sources 259 (2014) 25–32.
[28] F.K. Liu, S.Y. Hsieh, K. Fu-Hsiang, T.C. Chu, B.T. Dai, Jpn. J. Appl. Phys. Part 1 Regul. Pap. Short Notes Rev. Pap. 42 (2003) 4147–4151.
[29] M. Boutonnet, J. Kizling, P. Stenius, G. Maire, Colloids Surf. 5 (1982) 209–225.
[30] J. Hernández, J. Solla-Gullón, E. Herrero, J. Electroanal. Chem. 574 (2004) 185–196.
[31] R.W.J. Scott, O.M. Wilson, R.M. Crooks, J. Phys. Chem. B 109 (2004) 692–704.
[32] Y.-G. Kim, S.-K. Oh, R.M. Crooks, Chem. Mater. 16 (2003) 167–172.
[33] Y. Niu, L. Sun, R.M. Crooks, Macromolecules 36 (2003) 5725–5731.
[34] J.C. Garcia-Martinez, R.M. Crooks, J. Am. Chem. Soc. 126 (2004) 16170–16178.
[35] B.D. Cullity (Ed.), Elements of X-ray Diffraction, Addison-Wesley Publishing Company, Inc, London, 1978 second ed.
[36] T.J. Thomas, K.E. Ponnusamy, N.M. Chang, K. Galmore, S.D. Minteer, J. Membr. Sci. 213 (2003) 55–66.
[37] A.A. Karyakin, E.E. Karyakina, H.-L. Schmidt, Electroanalysis 11 (1999) 149–155.
[38] Y. Sun, Q. Ren, X. Liu, S. Zhao, Y. Qin, Biosens. Bioelectron. 39 (2013) 289–295.
[39] J.M. Goran, C.A. Favela, K.J. Stevenson, Anal. Chem. 85 (2013) 9135–9141.
[40] L.N. Pelster, M.T. Meredith, S.D. Minteer, Electroanalysis 24 (2012) 1011–1018.
[41] C.W. Narváez Villarrubia, R.A. Rincón, V.K. Radhakrishnan, V. Davis, P. Atanassov, ACS Appl. Mater. Interfaces 3 (2011) 2402–2409.